J|A|C|S
ARTICLES
Published on Web 12/11/2007

2-(4,5,6,7-Tetrafluorobenzimidazol-2-yl)-4,4,5,5-tetramethyl-4,5-dihydro-1-*H*-imidazole-3-oxide-1-oxyl, A Hydrogen-Bonded Organic Quasi-1D Ferromagnet

Hidenori Murata,[†,||] Yuji Miyazaki,[‡] Akira Inaba,[‡] Armando Paduan-Filho,[§] Valdir Bindilatti,[§] Nei Fernandes Oliveira Jr.,[§] Zeynep Delen,[†] and Paul M. Lahti*[,†]

Department of Chemistry, University of Massachusetts, Amherst, Massachusetts 01003, Research Center for Molecular Thermodynamics, Graduate School of Science, Osaka University, Toyonaka, Osaka 560-0043, Japan, and Instituto de Física, Universidade de São Paulo, Caixa Postal 66.318, 05315-970, São Paulo, SP, Brazil

Received June 9, 2007; E-mail: lahti@chem.umass.edu

Abstract: The title radical (F4BImNN) is a stable nitronylnitroxide that forms hydrogen-bonded NH···ON chains in the solid state. The chains assemble the F4BImNN molecules to form stacked contacts between the radical groups, in a geometry that is expected to exhibit ferromagnetic (FM) exchange based on spin polarization (SP) models. The experimental magnetic susceptibility of F4BImNN confirms the expectation, showing 1-D Heisenberg chain FM exchange behavior over 1.8−300 K with an intrachain exchange constant of $J_{chain}/k = +22$ K. At lower temperatures, ac magnetic susceptibility and variable field heat capacity measurements show that F4BImNN acts as a quasi-1-D ferromagnet. The dominant ferromagnetic exchange interaction is attributable to overlap between spin orbitals of molecules within the hydrogen-bonded chains, consistent with the SP model expectations. The chains appear to be antiferromagnetically exchange coupled, giving cusps in the ac susceptibility and zero field heat capacity at lower temperatures. The results indicate that the sample orders magnetically at about 0.7 K. The magnetic heat capacity ordering cusp shifts to lower temperatures as external magnetic field increases, consistent with forming a bulk antiferromagnetic phase below a Néel temperature of $T_N(0) = 0.72$ K, with a critical field of $H_c \approx 1800$ Oe. The interchain exchange is estimated to be $zJ/k \cong (-)0.1$ K.

Introduction

Purely organic molecular magnetic materials have been targets of continually increasing interest since they were proposed in the 1960s and realized in 1990s by discoveries of nitronylnitroxides and nitroxides that exhibit metal-free ferromagnetism at low temperatures, such as pNPNN.[1] There has been much effort to discern crystallographic structure−property relationships between intermolecular packing and magnetic behavior.[2] Hydrogen bonding has been a particularly promising strategy for attempting to control the crystallography of stable organic open-shell molecules and thereby their magnetic behaviors.[3]

We[4] and others[5−7] have had a strong interest in using benzimidazoles to organize organic radicals in magnetic systems. In particular, benzimidazoles readily form crystallographic

[†] University of Massachusetts.
[‡] Osaka University.
[§] Universidade de São Paulo.
[||] Present address: Department of Pure and Applied Chemistry, Faculty of Science and Technology, Tokyo University of Science, Noda, Chiba 278-8510, Japan.

(1) (a) Kinoshita, M.; Turek, P.; Tamura, M.; Nozawa, K.; Shiomi, D.; Nakazawa, Y.; Ishikawa, M.; Takahashi, M.; Awaga, K.; Inabe, T.; Maruyama, Y. *Chem. Lett.* **1991**, 1225. (b) Takahashi, M.; Turek, P.; Nakazawa, Y.; Tamura, M.; Nozawa, K.; Shiomi, D.; Ishikawa, M.; Kinoshita, M. *Phys. Rev. Lett.* **1991**, *67*, 746. (c) Tamura, M.; Nakazawa, Y.; Shiomi, D.; Nozawa, K.; Hosokoshi, Y.; Ishikawa, M.; Takahashi, M.; Kinoshita, M. *Chem. Phys. Lett.* **1991**, *186*, 401. (d) Turek, P.; Nozawa, K.; Shiomi, D.; Awaga, K.; Inabe, T.; Maruyama, Y.; Kinoshita, M. *Chem. Phys. Lett.* **1991**, *180*, 327. (e) Nakazawa, Y.; Tamura, M.; Shirakawa, N.; Shiomi, D.; Takahashi, M.; Kinoshita, M.; Ishikawa, M. *Phys. Rev.* **1992**, *B46*, 1. (f) Kinoshita, M. *Mol. Cryst. Liq. Cryst.* **1993**, *232*, 1. (g) Caneschi, A.; Ferraro, F.; Gatteschi, D.; le Lirzin, A.; Rentschler, E. *Inorg. Chim. Acta* **1995**, *235*, 159. (h) Caneschi, A.; Ferraro, F.; Gatteschi, D.; le Lirzin, A.; Novak, M. A.; Rentschler, E.; Sessoli, R. *Adv. Mater.* **1995**, *7*, 476. (i) Chiarelli, P.; Novak, M. A.; Rassat, A. *Nature* **1993**, *363*, 147.

(2) Some general references include: (a) Gatteschi, D., Kahn, O., Miller, J. S., Palacio, F., Eds. *Magnetic Molecular Materials*; Kluwer: Dordrecht, The Netherlands (1991). (b) Kahn, O. *Molecular Magnetism*; VCH: New York, 1993. (c) Iwamura, H.; Inoue, K.; Hayamizu, T. *Pure Appl. Chem.* **1996**, *68*, 243. (d) Veciana, J.; Cirujeda, J.; Rovira, C.; Molins, E.; Novoa, J. J. *J. Phys. I* **1996**, *6*, 1967. (e) Turnbull, M. M., Sugimoto, T., Thompson, L. K., Eds. *Molecule-Based Magnetic Materials. Theory, Techniques, and Applications*; American Chemical Society, Washington, DC, 1996. (f) Nakatsuji, S.; Anzai, H. *J. Mater. Chem.* **1997**, *7*, 2161. (g) Pilawa, B. *Ann. Phys.* **1999**, *8*, 191. (h) Lahti, P. M., Ed. *Magnetic Properties of Organic Materials*; Marcel Dekker: New York, 1999. (i) Itoh, K.; Kinoshita, M. *Molecular Magnetism: New Magnetic Materials*; Gordon and Breach: Newark, NJ, 2000. (j) Miller, J. S.; Drillon, M., Eds.: *Magnetism: Molecules to Materials*, Volumes I−III: Wiley-VCH: Weinheim, Germany, 2001. (k) Blundell, S. J.; Pratt, F. L. *J. Phys.: Condens. Matter* **2004**, *16*, R711. (l) Palacio F., Markova, T., Eds. *Carbon-based magnetism: An overview of the magnetism of metal-free carbon-based compounds and materials*; Elsevier: Amsterdam, The Netherlands, 2006.

(3) (a) Minguet, M.; Amabilino, D. B.; Vidal-Gancedo, J.; Wurst, K.; Veciana, J. *Mol. Cryst. Liq. Cryst. Sci. Technol., Sect. A* **1999**, *334*, 347. (b) Cirujeda, J.; Mas, M.; Molins, E.; Lanfranc de Panthou, F.; Laugier, J.; Park, J. G.; Paulsen, C.; Rey, P.; Rovira, C.; Veciana, J. *Chem. Commun.* **1995**, 709. (c) Cirujeda, J.; Hernandez-Gasio, E.; Rovira, C.; Stanger, J. L.; Turek, P.; Veciana, J. *J. Mater. Chem.* **1995**, *5*, 243. (d) Roques, N.; Maspoch, D.; Domingo, N.; Ruiz-Molina, D.; Wurst, K.; Tejada, J.; Rovira, C.; Veciana, J. *Chem. Commun.* **2005**, 4801. (e) Lahti, P. M. In *Carbon-based magnetism: An overview of the magnetism of metal-free carbon-based compounds and materials*; Makarova, T., Palacio, F., Eds.; Elsevier: Amsterdam, 2006; p 23ff.

 10.1021/ja074211g CCC: $40.75

chains due to their 1-D NH donor to azole N acceptor NH···N interactions and offer a convenient crystallographic scaffolding to try to arrange attached radicals. Ferrer et al.[4a] and Miyazaki et al.[4e] reported magnetostructural and calorimetric studies showing 2-*tert*-butylnitroxylbenzimidazole (BABI) to be an antiferromagnet with a Néel temperature of 1.7 K. Yoshioka and co-workers have reported magnetostructural studies of 2-(benzimidazol-2-yl)-4,4,5,5-tetramethyl-4,5-dihydro-1*H*-imidazole-3-oxide-1-oxyl (BImNN) showing it to exhibit strong 1-D chain ferromagnetic (FM) exchange interactions.[5a−c] Additional studies on BImNN by Blundell and co-workers confirmed the dominance of 1-D FM chain interactions and suggested the presence of additional interchain exchange interactions.[7]

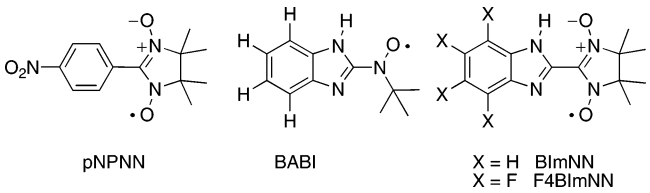

Some of us recently reported that 2-(4,5,6,7-tetrafluorobenzimidazol-2-yl)-4,4,5,5-tetramethyl-4,5-dihydro-1*H*-imidazole-3-oxide-1-oxyl (F4BImNN) shows strong 1-D chain ferromagnetic (FM) exchange that is quite similar to that of BImNN.[4g] This showed that two molecules (BImNN and F4BImNN) having similar shapes, similar placement of similar hydrogen bonding donor and acceptor groups, but strong electronic perturbation of the polarity of substituent groups (F for H substitutions on the benzenoid ring) can still yield similar crystal packing with commensurately similar magnetic behavior. Also, an organic alloy of BImNN and F4BImNN gives similar 1-D crystallographic chain formation and 1-D FM exchange interactions to the behaviors noted for the pure constituent radicals.[4h] It was not obvious that there would be strong crystallographic similarities between BImNN and F4BImNN (or their organic alloys), given that fluorination can induce large changes in molecular properties. Indeed, Yoshioka's group has found that a number of other BImNN structural analogues are quite different from BImNN in magnetic and crystallographic behavior.[5d−h]

The preliminary report[4g] about F4BImNN noted that, despite the similarity of crystallography and magnetism to those of BImNN, the crystallographic packing was not identical. Because subtle changes in molecular packing can give significant changes in magnetic behavior, further study of F4BImNN seemed appropriate. This article gives full details of the synthesis and magnetostructural analysis of F4BImNN, including new magnetic and calorimetric studies that show it to act as a quasi 1-D organic ferromagnet whose strongly FM coupled, hydrogen-bonded chains are antiferromagnetically coupled to give magnetic ordering below a critical temperature of about 0.7 K.

Experimental Section

General Methods. Ethanol (anhydrous, water <0.02%) and methanol (anhydrous, water <0.01%) were dried over 3 Å molecular sieves before use. Triethylamine (99%) and chloroform (HPLC grade) were obtained from Fisher Scientific and used as received. Other reagents were used as received.

Instrumental Analyses. All melting points are reported uncorrected. Mass spectrometry was carried out at the University of Massachusetts Amherst Mass Spectrometry Facility, which is supported in part by the National Science Foundation. Solution-phase electronic spin resonance experiments were carried out at room temperature, using a Bruker Biospin Elexsys E-500 spectrometer system. Samples were dissolved in spectro-grade toluene, placed in 4 mm o.d. quartz tubes, subjected to freeze−pump−thaw degassing and measured at 9.6 GHz, modulation frequency 100 MHz, and modulation amplitude 0.05 G.

DC magnetization and AC susceptibility measurements between 1.8 and 300 K were carried out on crushed polycrystalline samples of F4BImNN placed in gelatin capsules and held in place with a small amount of cotton. The samples were placed in a plastic straw and inserted into a Quantum Design MPMS-5 SQUID magnetometer. The magnetic behavior was measured at various applied fields (1000−50 000 Oe).

AC susceptibility measurements between 0.5 and 4.2 K were carried out by the mutual inductance method, using polycrystalline samples in polyvinylchloride sample holders. The experimental setup is described elsewhere.[8]

Heat capacity measurements under a magnetic field were carried out with a commercial calorimeter based on a relaxation method (Quantum Design, PPMS 6000). To verify the absolute heat capacity values, adiabatic calorimetry measurements were also done using a laboratory-made apparatus that is described elsewhere.[9]

Crystallographic analyses were carried out at the University of Massachusetts Chemistry Department X-ray Structural Characterization Facility (NSF CHE-9974648) on a Bruker Nonius CCD instrument. Data workup was carried out using SHELXTL[10] and PLATON.[11] ORTEP diagrams were generated using ORTEP-3 for Windows.[12]

(4) (a) Ferrer, J. R.; Lahti, P. M.; George, C.; Antorrena, G.; Palacio, F. *Chem. Mater.* **1999**, *11*, 2205. (b) Xie, C.; Lahti, P. M. *Tetrahedron Lett.* **1999**, *40*, 4305. (c) Ferrer, J. R.; Lahti, P. M.; George, C.; Oliete, P.; Julier, M.; Palacio, F. *Chem. Mater.* **2001**, *13*, 2447. (d) Lahti, P. M.; Ferrer, J. R.; George, C.; Oliete, P.; Julier, M.; Palacio, F. *Polyhedron* **2001**, *20*, 1465. (e) Miyazaki, Y.; Sakakibara, T.; Ferrer, J. R.; Lahti, P. M.; Antorrena, G.; Palacio, F.; Sorai, M. *J. Phys. Chem. B* **2002**, *106*, 8615. (f) Delen, Z.; Xie, C.; Hill, P. J.; Choi, J.; Lahti, P. M. *Cryst. Growth Des.* **2005**, *5*, 1867. (g) Murata, H.; Delen, Z.; Lahti, P. M. *Chem. Mater.* **2006**, *18*, 2625. (h) Murata, H.; Mague, J. T.; Aboaku, S.; Yoshioka, N.; Lahti, P. M. *Chem. Mater.* **2007**, *19*, 4111.

(5) (a) Yoshioka, N.; Irisawa, M.; Mochizuki, Y.; Aoki, T.; Inoue, H. *Mol. Cryst. Liq. Cryst. Sci. Technol., Sect. A* **1997**, *306*, 403. (b) Yoshioka, N.; Irisawa, M.; Mochizuki, Y.; Kato, T.; Inoue, H.; Ohba, S. *Chem. Lett.* **1997**, 251. (c) Yoshioka, N.; Inoue, H. Crystal Control in Organic Radical Solids. In *Magnetic Properties of Organic Materials*; Lahti, P. M., Ed.; Marcel Dekker: New York, 1999; p 553. (d) Yoshioka, N.; Matsuoka, N.; Irisawa, M.; Ohba, S.; Inoue, H. *Mol. Cryst. Liq. Cryst. Sci. Technol., Sect. A* **1999**, *334*, 239. (e) Nagashima, H.; Irisawa, M.; Yoshioka, N.; Inoue, H. *Mol. Cryst. Liq. Cryst. Sci. Technol., Sect. A* **2002**, *376*, 371. (f) Nagashima, H.; Hashimoto, N.; Inoue, H.; Yoshioka, N. *New J. Chem.* **2003**, *27*, 805. (g) Nagashima, H.; Inoue, H.; Yoshioka, N. *Polyhedron* **2003**, *22*, 1823. (h) Nagashima, H.; Fujita, S.; Inoue, H.; Yoshioka, N. *Cryst. Growth Des.* **2004**, *4*, 19.

(6) (a) Fegy, K.; Sanz, N.; Luneau, D.; Belorizky, E.; Rey, P. *Inorg. Chem.* **1998**, *37*, 4518. (b) Fegy, K.; Luneau, D.; Ohm, T.; Paulsen, C.; Rey, P. *Angew. Chem., Int. Ed.* **1998**, *37*, 1270. (c) Lescop, C.; Luneau, D.; Belorizky, E.; Fries, P.; Guillot, M.; Rey, P. *Inorg. Chem.* **1999**, *38*, 5472. (d) Lescop, C.; Luneau, D.; Bussiere, G.; Triest, M.; Reber, C. *Inorg. Chem.* **2000**, *39*, 3740. (e) Liu, Z.-L.; Zhao, B.; Jiang, Z.-H.; Yan, S.-P. *Gaodeng Xuexiao Huaxue Xuebao* **2001**, *22*, 5. (f) Beaulac, R.; Bussiere, G.; Reber, C.; Lescop, C.; Luneau, D. *New J. Chem.* **2003**, *27*, 1200.

(7) (a) Sugano, T.; Blundell, S. J.; Hayes, W.; Day, P. *Polyhedron* **2003**, *22*, 2343. (b) Sugano, T.; Blundell, S. J.; Hayes, W.; Day, P. *J. Phys. IV: Proceedings* **2004**, *114*, 651. (c) Sharmin, S.; Blundell, S. J.; Sugano, T.; Ardavan, A. *Polyhedron* **2005**, *24*, 2360.

(8) Oliveira, N. F., Jr.; Paduan-Filho, A.; Salinas, S. R.; Becerra, C. C. *Phys. Rev. B* **1978**, *18*, 6165.

(9) Kume, Y.; Miyazaki, Y.; Matsuo, T.; Suga, H. *J. Phys. Chem. Solids* **1992**, *53*, 1297.

(10) Sheldrick, G. M. *SHELXTL97 Program for the Refinement of Crystal Structures*; University of Göttingen: Germany, 1997.

(11) Spek, A. L. *J. Appl. Crystallogr.* **2003**, *36*, 7−13.

(12) Farrugia, L. J. *J. Appl. Crystallogr.* **1997**, *30*, 565.

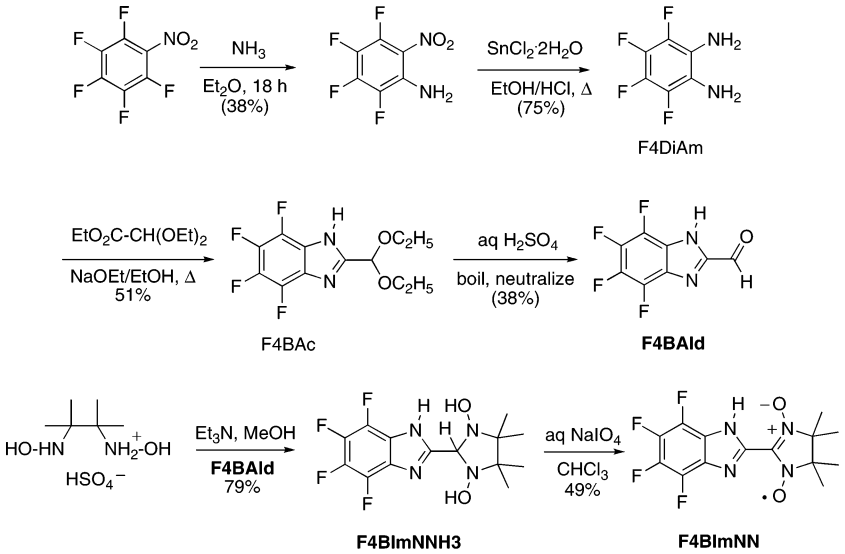

Figure 1. Synthesis of F4BImNN.

2,3-Bis(hydroxylamino)-2,3-dimethylbutane hydrogen sulfate was prepared from 2-nitropropane according to the procedure of Ovcharenko et al.[13]

3,4,5,6-Tetrafluoro-1,2-phenylenediamine (F4DiAm) was prepared from commercially available nitropentachlorobenzene (Aldrich) according to the procedure of Heaton et al.[14]

4,5,6,7-Tetrafluorobenzimidazole-2-carbaldehyde Diethyl Acetal (F4BAc). Sodium (0.483 g, 21.0 mmol) was carefully added to dry ethanol (12 mL) followed by 3,4,5,6-tetrafluoro-1,2-phenylenediamine (1.60 g, 8.88 mmol) and ethyl diethoxyacetate (2.11 g, 12.0 mmol). The mixture was heated at reflux for 24 h and cooled to room temperature, and then the solvent was removed under vacuum. The residue was dissolved in water and extracted with dichloromethane. The organic layer was separated to dryness. Chromatography on silica gel with ethyl acetate/hexane (3/7) as the eluent yielded the acetal (1.48 g, 51%) as a white powder. Mp: 208−209 °C. ^{1}H NMR (400 MHz, $CDCl_3$, ppm): δ 11.19 (br s, 1H, NH), 5.74 (s, 1H, CH), 3.68 (m, 4H, CH_2), 1.17 (t, 6H, J = 7.0 Hz, CH_3). IR (KBr pellet, cm^{-1}): 2930 (NH str). MS (EI): calcd for $C_{12}H_{12}N_2F_4O_2$ m/z = 292.2. Found m/z = 292. Elemental analysis calcd for $C_{12}H_{12}N_2F_4O_2$: C, 49.30; H, 4.14; N, 9.59. Found: C, 49.53; H, 4.16; N, 9.51.

4,5,6,7-Tetrafluorobenzimidazole-2-carbaldehyde (F4BAld). A solution of 4,5,6,7-tetrafluorobenzimidazole-2-carboxaldehyde diethyl acetal (1.34 g, 4.59 mmol) in 1 M aqueous sulfuric acid (300 mL) was stirred for 1 h at room temperature and then boiled for 10 min. The solution was cooled to room temperature, and the pH was adjusted to ca. 9 with aqueous sodium carbonate. The resulting precipitate was filtered, washed with water, and dried under vacuum to yield the product (0.766 g, 77%) as a white powder. Mp: 206−207 °C. ^{1}H NMR (400 MHz, acetone-d_6, ppm): δ 9.99 (s, 1H, CHO). IR (KBr pellet, cm^{-1}): 3076 (NH str), 1700 (C=O str). MS (EI): calcd for $C_8H_2N_2F_4O$ m/z = 218.1. Found m/z = 218. Elemental analysis calcd for $C_8H_2N_2F_4O$: C, 44.10; H, 0.92; N, 12.80. Found: C, 42.81; H, 1.00; N, 12.56.

2-(4,5,6,7-Tetrafluorobenzimidazol-2-yl)-1,3-dihydroxy-4,4,5,5-tetramethylimidazolidine (F4BImNNH3). 2,3-Bis(hydroxylamino)-2,3-dimethylbutane hydrogen sulfate (0.692 g, 2.81 mmol) and 4,5,6,7-tetrafluorobenzimidazole-2-carbaldehyde (0.613 g, 2.81 mmol) were dissolved in 21 mL of HPLC-grade methanol. To this mixture was added triethylamine (0.284 g, 2.81 mmol). The mixture was stirred for 48 h under argon at room temperature and filtered. The resulting white solid was washed with ice-cold methanol and dried to give the product (0.772 g, 79%) as a white solid. Mp: 176−177 °C (decomp). ^{1}H NMR (400 MHz, acetone-d_6, ppm): δ 12.04 (br s, 1H, NH), 5.10 (s, 1H, CH), 1.19 (s, 6H, CH_3), 1.17 (s, 6H, CH_3). IR (KBr pellet, cm^{-1}): 3285 (OH str), 2943 (NH str). MS (EI): calcd for $C_{14}H_{16}N_4F_4O_2$ m/z = 348.3. Found m/z = 348. Elemental analysis calcd for $C_{14}H_{16}N_4F_4O_2$: C, 48.30; H, 4.63; N, 16.10. Found: C, 49.42; H, 5.16; N, 14.08.

2-(4,5,6,7-Tetrafluorobenzimidazol-2-yl)-4,4,5,5-tetramethy-4,5-dihydro-1*H*-imidazole-3-oxide-1-oxyl (F4BImNN). To a suspension of 2-(4,5,6,7-tetrafluorobenzimidazol-2-yl)-1,3-dihydroxy-4,4,5,5-tetramethylimidazolidine (0.624 g, 1.79 mmol) in 75 mL of chloroform were added 76 mL of 0.25 M aqueous sodium periodate (1.90 mmol). A deep blue color formed as soon as the oxidizing solution was added. The mixture was stirred at room temperature under argon for 10 min. The chloroform layer was separated, and the aqueous layer was extracted with chloroform. The combined organic layers were dried over anhydrous calcium chloride and evaporated to dryness. Chromatography on silica gel with ethyl acetate/hexane (1/1) yielded the product (0.305 g, 49%), which was recrystallized from chloroform/methanol to give crystallographic quality, shiny blue-black prisms. Mp: 170−172 °C (decomposition). ESR (toluene, 9.63086 GHz): 7.22 G (2 N). IR (KBr pellet, cm^{-1}): 3396 (NH, str). MS (EI): calcd for $C_{14}H_{13}N_4F_4O_2$ m/z = 345.1, found m/z = 345. Elemental analysis calcd for $C_{14}H_{13}F_4N_4O_2$: C, 48.70; H, 3.80; N, 16.22; F, 22.01. Found: C, 49.27; H, 3.99; N, 15.71; F, 22.00. Single-crystal X-ray diffraction analysis details were deposited with the Cambridge Crystallographic Database, CCDC No. 295499.

Results and Discussion

Synthesis and Characterization. The synthesis of F4BImNN is summarized in Figure 1. The procedure of Heaton et al.[14] was used to make diamine F4DiAm in good yield. The diamine was then condensed with ethyl diethoxyacetate to give acetal F4BAc and deprotected to the corresponding aldehyde F4BAld. The aldehyde was condensed with 2,3-bis(hydroxylamino)-2,3-dimethylbutane hydrogen sulfate[13] in the presence of triethylamine to make the bis-hydroxylamine precursor of the desired radical, F4BImNNH3. Oxidation with aqueous sodium periodate followed by column chromatography gave crude F4BImNN, which can be recrystallized to give large blue-black prisms that are highly stable to ambient conditions. This sequence works sufficiently well that synthesis of up to a 0.5 g of radical is readily accomplished.

(13) Ovcharenko, V.; Fokin, S.; Rey, P. *Mol. Cryst. Liq. Cryst. Sci. Technol., Sect. A* **1999**, *334*, 109.
(14) Heaton, A.; Hill, M.; Draksmith, F. *J. Fluorine Chem.* **1997**, *81*, 133.

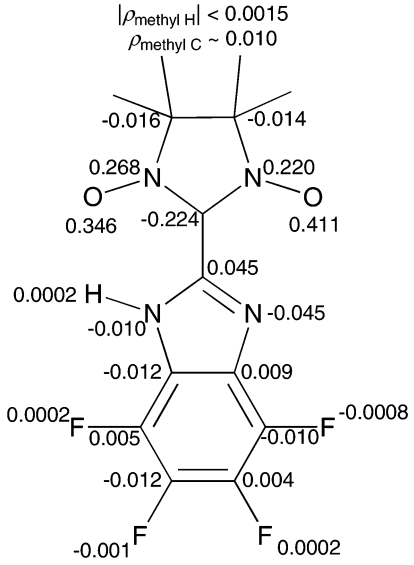

Figure 2. Spin populations (ρ_{spin}) of F4BImNN computed at UB3LYP/LANL2DZ level of theory using crystallographic geometry.

Electron spin resonance (ESR) spectroscopy of F4BImNN in toluene solution at room temperature shows a typical pentet pattern hyperfine coupling (hfc) of 7.2 G from two equivalent nitrogens. Computational estimates of the spin density populations at the UB3LYP/LANL2DZ level of theory[15,16] are given in Figure 2, based on the F4BImNN crystal structure described below. The major computed spin density is on the nitronylnitroxide N−O groups, consistent with experiment. The qualitative spin distribution follows π-spin polarization (SP) expectations, except for the nonalternant imidazole unit, and the same-sign polarization of fluorines as the benzenoid π-carbons to which they are attached. The computations show significant spin density on the imidazole unit, but this was not resolved in the experimental ESR spectra.

Figure 3 shows solid polycrystalline ESR spectra of F4BImNN as temperature decreases. The spectral g_{avg} determined from the absorption mode maxima decreases sharply at lower temperatures, consistent with changes in the g-tensor in low dimensional magnetic systems having dominant exchange along one crystallographic axis.[17] The spectra split to exhibit multiple features with cooling, and the spectral extent becomes broad, especially below about 25 K. These temperature variations are all reversible. Qualitatively similar changes were observed by Sharmin et al.[7c] in ESR studies of BImNN single crystals. They also noted the appearance of additional transitions in the ESR spectrum at lower temperatures, which they tentatively ascribed either to a structural phase transition or an onset of hyperfine structure features in their spectra.

Table 1 summarizes the X-ray diffraction analysis of a single crystal of F4BImNN. Figure 4 shows an ORTEP style representation of the structure. The most notable features of the crystal packing are the hydrogen-bonded chains where the N−H units are donors and both radical O−N and azole N act to some degree as acceptors, as shown in Figure 5. This chain motif is

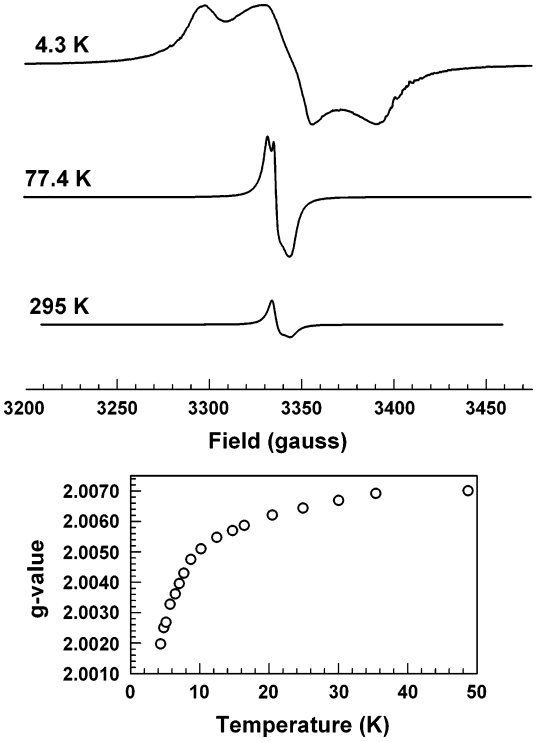

Figure 3. Selected polycrystalline solid ESR spectra and temperature dependence of g_{avg} of F4BImNN. The spectral ordinate scales are the same.

Table 1. Crystallographic Summary for F4BImNN, CCDC No. 295499

Crystal Data	
formula	$C_{14}H_{13}F_4N_4O_2$
formula weight	345.2
crystal system	monoclinic
space group	*P*21/*c* (no. 14)
a, *b*, *c* [Å]	8.6540(4), 20.9710(9), 8.8500(4)
α, β, γ [deg]	90, 110.397(2), 90
V [Å^3]	1505.42(12)
Z	4
D(calc) [g/cm^3]	1.523
Mu(Mo Kα) [mm^{-1}]	0.138
F(000)	708
crystal size [mm^3]	0.01 × 0.03 × 0.09
Data Collection	
temperature (K)	293
radiation [Å, Mo Kα]	0.710 73
θ (min, max) [deg]	1.9, 25.0
dataset ($-h$, h; $-k$,k; $-l$,l)	−10, 10; −24, 24; −10, 10
tot., uniq. data, *R*(int)	5128, 2653, 0.031
observed data [$I > 2\sigma(I)$]	1783
Refinement	
N_{ref}, N_{par}	2653, 219
$R(I > 2\sigma)$, $wR(I > 2\sigma)$	0.0517, 0.1613
R(all), wR_2(all)	0.0863, 0.1932
S(all)	1.16
min, max resd density [e/Å^3]	−0.24, 0.27

analogous to that in BImNN.[5a−c] Table 2 shows important intermolecular, intrachain contacts generated by the symmetry operation (x, $^1/_2 - y$, $^1/_2 + z$). The double dashed line in Figure 5 shows the (N)H···O hydrogen bond contact, with a fairly short (N1)H1···O2_4 distance of 2.01 Å (r(N1···O2) = 2.814(4) Å). The (N1)H1···N2_4 contact of about 2.7 Å ((r(N1···N2) = 3.152(4) Å)) shown by the dashed single line in the figure is significantly longer; its length indicates that it is weaker than the (N1)H1···O2_4 interaction. Both contacts are also signifi-

(15) (a) Lee, C.; Yang, W.; Parr, R. G. *Phys. Rev. B* **1988**, *37*, 785. (b) Becke, A. D. *J. Chem. Phys.* **1993**, *98*, 5648. (c) Stephens, P. J.; Devlin, F. J.; Chabalowski, C. F.; Frisch, M. J. *J. Phys. Chem.* **1994**, *98*, 11623.
(16) Computations were carried out using Gaussian 03, rev B.03: Frisch, M. J., et al. Gaussian Inc.: Pittsburgh, PA, 2003.
(17) Nagata, K.; Tazuke, Y. *J. Phys. Soc. Jpn.* **1972**, *32*, 337.

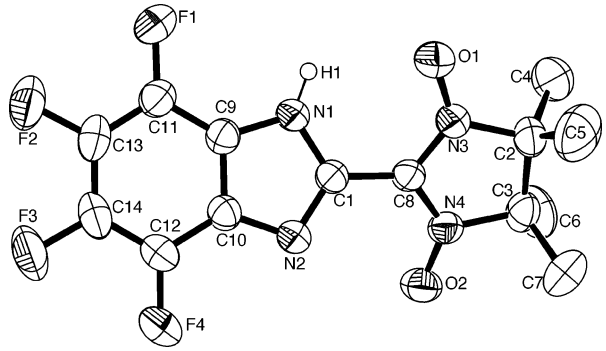

Figure 4. ORTEP diagram for F4BImNN showing 50% probability ellipsoids.

cantly bent by comparison to the ideal of linearity for hydrogen bonds (155° for N1−H1···O2_4, and 110° for N1−H1···N2_4), but both probably contribute to forming the chains in Figure 5.

Magnetic Measurements. Figure 6 shows the results of static field, dc magnetic susceptibility measurements ($\chi = M/H$) at 1000 Oe for polycrystalline F4BImNN, plotted as χT over 1.8−300 K. The increase in χT to about 3.0 emu·K/Oe·mol as temperature decreases to 1.8 K shows the presence of ferromagnetic (FM) exchange interactions. F4BImNN is prone to susceptibility saturation,[5g] like BImNN,[7a] but magnetization vs field measurements at 1.8 K (Figure 7) show a nearly linear response up to 1000 Oe. The inset of Figure 6 shows the lower temperature portion of a Curie−Weiss plot of the data as $1/\chi$ versus T. A linear fit of the higher temperature portion of the data gives a Curie constant of 0.389 emu·K/Oe·mol and a Weiss intercept of $\theta = (+)11$ K. The Curie constant is in good accord with the value expected for $S = {}^1/_2$ spin carriers, and the Weiss constant shows that there are quite strong FM exchange interactions for an organic solid.

The χT data can be fit to a 1-D Heisenberg FM chain model using the Hamiltonian in eq 1, where the exchange constant J is the intrachain exchange constant between neighboring molecules i and j

$$H = -2J \sum S_i \cdot S_j \qquad (1)$$

From eq 1, the susceptibility dependence on temperature for isolated 1-D ferromagnetic chains is given by eq 2:[18−19]

$$\chi = \frac{Ng^2\mu_B{}^2}{4kT} \cdot \left[\frac{1 + A \cdot x + B \cdot x^2 + C \cdot x^3 + D \cdot x^4 + E \cdot x^5}{1 + F \cdot x + G \cdot x^2 + H \cdot x^3 + I \cdot x^4} \right]^{2/3} + \text{TIC}$$

$$x = J/(2kT)$$

$$A = 5.797\,991\,6,\ B = 16.902\,653,$$
$$C = 29.376\,885,\ D = 29.832\,959,\ E = 14.036\,918$$
$$F = 2.797\,991\,6,\ G = 7.008\,678\,0,$$
$$H = 8.653\,864\,4,\ I = 4.574\,311\,4 \qquad (2)$$

where the various physical constants have their usual meanings. The Landé constant for F4BImNN was fixed at $g = 2.0066$ from the room-temperature polycrystalline ESR measurements; the exchange constant $J_{chain}/k = J/k$ and the TIC (temperature independent correction) were optimized by a nonlinear fit to the data. Figure 6 shows the data and the fitted curve, where both are shown after correction for the TIC: the fitted $J_{chain}/k = (+)22.1 \pm 0.6$ K, where the uncertainty is the statistical 95% confidence limits. Sugano et al.[7a] reported $J_{chain}/k = (+)22$ K for BImNN, measuring magnetic susceptibility at 200 Oe to limit saturation effects. The intrachain exchange strengths for BImNN and F4BImNN are thus very similar, consistent with the similarities of the crystallographic chains in these systems.

The molar magnetization of F4BImNN easily saturates at 1.8 K, as shown in Figure 7. The experimental saturation magnetization $M_{sat} \approx 5400$ emu/mol from the high field region is compatible with expectations for $S = {}^1/_2$ spin per radical. But, the experimental $M(H)$ curve is most consistent with an effective spin quantum number of $S_{eff} \approx 9$ using eq 3, where $B(y)$ is a Brillouin function of magnetic field H and spin quantum number $S = S_{eff}$. A comparison of the theoretical $S_{eff} = 9$ magnetization curve at 1.8 K to the data is given in Figure 7, normalized to the experimental M_{sat}. Thus, S_{eff} is much larger than the value expected for nearly isolated $S = {}^1/_2$ F4BImNN spin carriers. This is due to the strong exchange between radicals.

$$M = N\mu_B\, g \cdot S \cdot B(y)$$
$$B(y) = \frac{2S+1}{2S} \coth\left(\frac{2S+1}{2S} y\right) - \frac{1}{2S} \coth\left(\frac{y}{2S}\right)$$
$$y = \frac{g\mu_B \cdot S \cdot H}{kT} \qquad (3)$$

The ac susceptibility behavior of F4BImNN was also measured in a number of experiments. Figure 8 shows χ_{ac} data for F4BImNN obtained at several external fields from 0 to 7000 Oe, all at 50 Hz modulation frequency and 1 Oe modulation field, between 2.1 and 10.0 K. No significant imaginary component to the χ_{ac} was found under any of these conditions. As the figure shows, χ_{ac} exhibits field dependent maxima. These results are virtually the same at modulation frequencies of 17 and 1500 Hz, so the χ_{ac} peak maximum positions are static rather than dynamic in behavior (independent of ac modulation frequency.) This behavior arises from short-range fluctuations in the magnetization[20] and indicates a crossover between low temperature behavior dominated by the temperature proximity of an ordered phase and the high temperature behavior of the paramagnetic phase.

Idealized, completely isolated 1-D FM chains should not show ordering above absolute zero.[21] But, experimentally realistic systems with even small interchain interactions can give a magnetically ordered state. Therefore the magnetic behavior of F4BImNN was investigated below 2 K using a ^{3}He refrigerator system.[8] Figure 9 shows the χ_{ac} data obtained at zero applied field, 155 Hz modulation frequency, 10 Oe modulation field, over 0.5−4.1 K. The data exhibit a characteristic λ-shaped cusp at 0.72 K, consistent with bulk magnetic ordering.

Heat Capacity Measurements. Thermochemical measurements were carried out on polycrystalline samples of F4BImNN to investigate the nature of its ordering transition. Figure 10 shows heat capacity measurements C_p as a function of temperature at zero field and at multiple external applied magnetic fields up to 20 000 Oe. The zero-field results show an ordering

(18) Baker, G. A., Jr.; Rushbrooke, G. S.; Gilbert, H. E. *Phys. Rev.* **1964**, *135*, A1272.
(19) Swank, D. D.; Landee, C. P.; Willet, R. D. *Phys. Rev. B* **1979**, *20*, 2154.
(20) Becerra, C. C.; Paduan-Filho, A. *Solid State Commun.* **2003**, *125*, 99.
(21) Ising, E. *Z. Phys.* **1925**, *31*, 253.

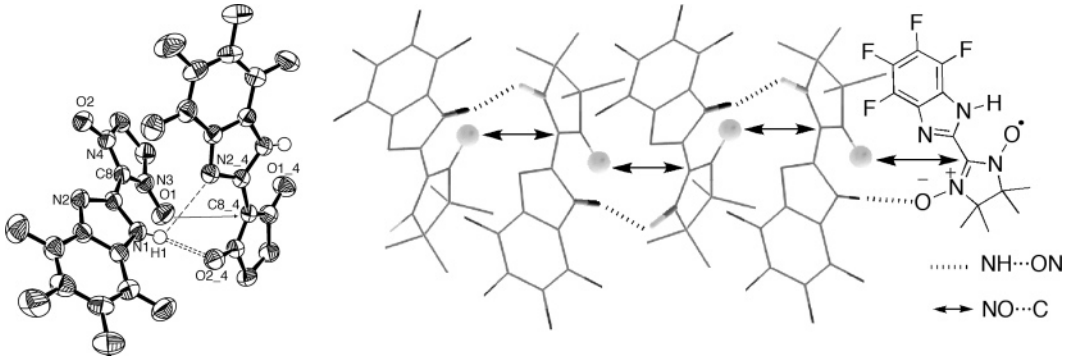

Figure 5. Intermolecular chain contacts for F4BImNN. Methyl groups are omitted in the ORTEP view for clarity. See Table 2 for contact distances.

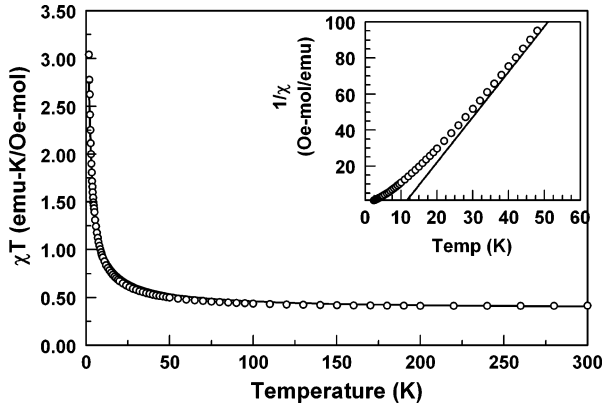

Figure 6. χT versus temperature data for F4BImNN at 1000 Oe, corrected for temperature-independent magnetism. Solid line in main chart shows 1-D Heisenberg chain fit to data using eq 2. Solid line in inset shows Curie−Weiss line extrapolated from higher temperature $1/\chi(T)$ data.

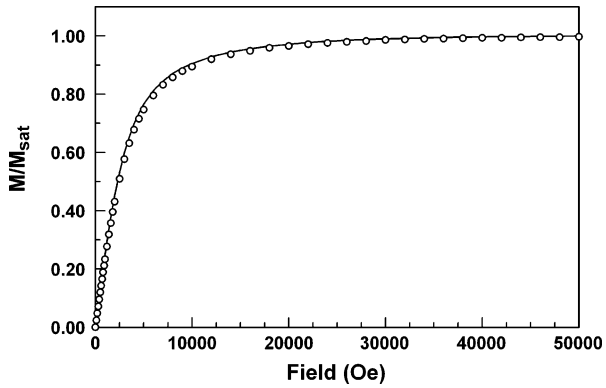

Figure 7. Magnetization versus field data at 1.8 K for F4BImNN. The solid line shows eq 3 for $T = 1.8$ K, $S = 9$; the data and the curve have been normalized to the experimental M_{sat}.

Table 2. Selected Intrachain Intermolecular Distances (Å) for F4BImNN; See Figure 5

O1···C8_4	3.139(4)	O1···N4_4	3.024(4)
O1···O2_4	3.165(4)	O1···N2_4	3.198(4)
N1···O2_4	2.814(4)	H1···O2_4	2.01
N1···N2_4	3.152(4)	H1···N2_4	2.75

cusp anomaly at 0.72 K, in good accord with the results from the ac magnetic measurements.

Equation 4 from mean field theory yields a rough estimate of the magnitude of interchain exchange $|zJ_{inter}|$ between the strongly FM exchange coupled chains, where z is the (here unspecified) number of neighboring sites interacting with the chain. Using $J_{chain}/k = +22$ K from above, the observed $T_c = 0.7$ K yields $|zJ_{inter}/k| = 0.09$ K for $S = {}^1/_2$ spin carriers.

$$T_c \approx 2S^2(|zJ_{inter}| \cdot J_{chain})^{1/2} \quad (4)$$

The changes in the critical temperature cusp in the magnetic C_p data with increasing external field are similar to the behavior

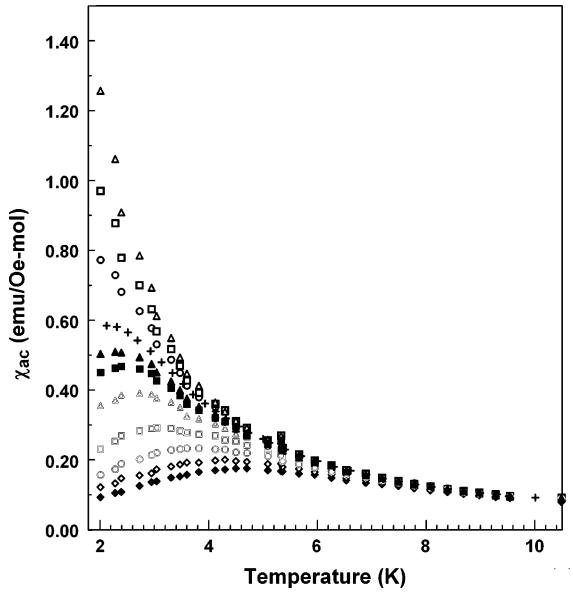

Figure 8. Field-cooled ac magnetic susceptibility for F4BImNN at 50 Hz modulation frequency, 1 Oe modulation field, and constant applied fields as follows: 0 Oe (△, upper), 1000 Oe (□, upper), 1500 Oe (○, upper), 2000 Oe (+), 2250 Oe (▲), 2500 Oe (■), 3000 Oe (△), 4000 Oe (□), 5000 Oe (○), 6000 Oe (◇), 7000 Oe (◆).

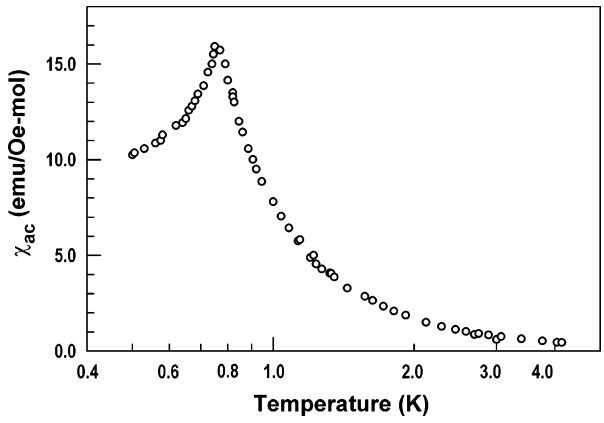

Figure 9. Ac magnetic susceptibility for F4BImNN at zero field, 155 Hz modulation frequency, 10 Oe modulation field.

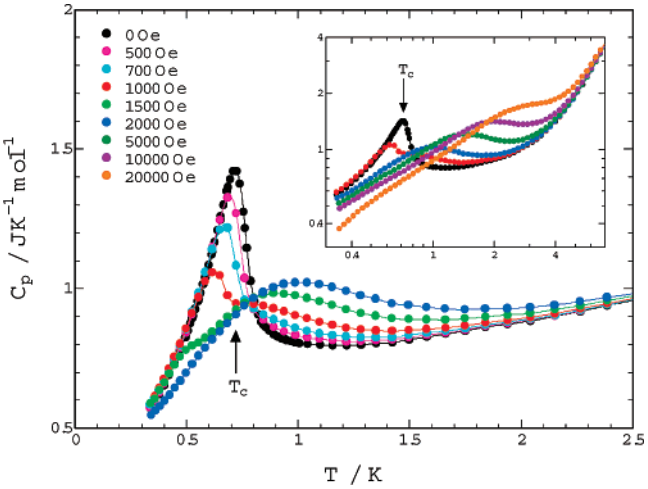

Figure 10. Experimental heat capacity for F4BImNN at several external magnetic fields versus temperature.

of other quasi-1D ferromagnetic systems having very weak interchain exchange interactions, such as 3(4-chlorophenyl)-1,5-diphenyl-6-oxoverdazyl, CDVO.[22] In particular, the behavior is consistent with formation of a ground state bulk antiferromagnetic phase below T_c. This is also consistent with the fact that χ_{ac} for polycrystalline F4BImNN at the lowest measured temperature approaches two-thirds of its maximum value at the T_c cusp. For an antiferromagnet, eq 5 gives the relationship expected[23] between the Néel temperature $T_c = T_N$ and the applied external magnetic field, where all terms have the typical meanings. The T_c versus field data from Figure 10 give a good fit to eq 5 as shown in Figure 11 for $T_c(0) = T_N(0) = 0.717 \pm 0.001$ K, critical field $H_c = 1.81 \pm 0.07$ kOe, and coefficients $\alpha = 1.7 \pm 0.1$, $\xi = 0.31 \pm 0.05$; the uncertainties are statistical 95% confidence limits. The interchain exchange interaction estimated from H_c using eq 6 with $g = 2.0066$ (from the ESR studies above) is $zJ_{inter}/k = (-)0.12$ K. This is in good accord with the mean field estimated magnitude obtained from T_c and J_{chain}/k using eq 4.

$$T_N(H) = T_N(0)[1 - (H/H_c)^{\alpha}]^{\xi} \quad (5)$$

$$H_c \approx (2|zJ_{inter}| \cdot S^2/g\mu_B)^{1/2} \quad (6)$$

Interestingly, the C_p data below the ordering cusp (where the lattice contribution is very small) are proportional to $T^{3/2}$. According to spin wave theory,[24] a $C_p \approx T^{3/2}$ dependence is more consistent[25−26] with ferromagnetic ordering below T_c, while $C_p \approx T^3$ dependence is expected[26] for antiferromagnets.

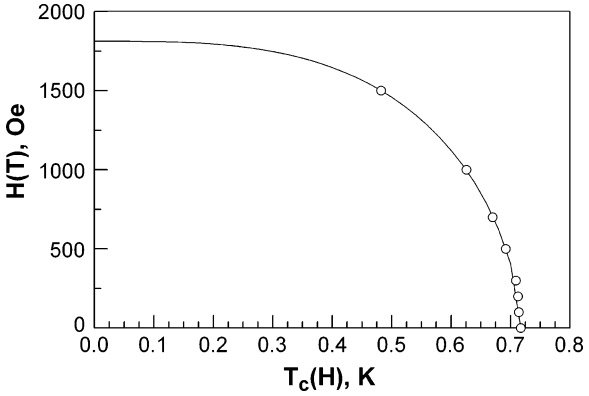

Figure 11. T_c-H phase diagram from data in Figure 10. Solid line is a fit to eq 6; see the text for details.

Previous work has suggested some reasons for $T^{3/2}$ dependence of the low temperature heat capacity when magnetic studies indicate antiferromagnetic ordering.[26] At present, it is clear that F4BImNN forms an ordered state below T_c, and the variation in T_c with the external field is consistent with a low dimensional magnet having strongly anisotropic 1-D FM chain type exchange and weak AFM exchange between the chains. Further details of the nature of the ordered state are under investigation.

Magnetostructural Considerations. Yoshioka has described[5a−c] the most likely exchange path governing FM exchange in BImNN, which presumably also applies to the crystallographically similar F4BImNN. The F4BImNN hydrogen bond scaffolding assembles molecules into 1-D stacks in which radical N−O groups have excellent intermolecular overlap with the central carbon in neighboring nitronylnitroxide groups. Figure 12 shows spin density isosurface maps[16] of high spin FM and low spin AFM exchange coupled states of a pair of molecules from the stack, with z-clipping at a plane that shows the N−O···C contact shown in the simplified structural inset. The computations were done using spin-unrestricted B3LYP hybrid density functionals with a 6-31G* basis set (Gaussian[16] keyword Guess = Mix for the $S = 0$ state); the methyl groups were replaced with hydrogen atoms on the nitronylnitroxide unit. The favorable contact with the opposite sign of spin density is readily apparent in the high spin FM state (green···blue N−O···C contact), while unfavorable contact between sites with the same sign (green···green) occurs in the AFM state. The observed FM 1-D chain type magnetic exchange is thus completely consistent with the expectations of a SP model following N−O···C contacts as shown in Figure 13.

If exchange followed the hydrogen bond contacts by an SP pathway instead, AFM chain exchange would be expected (Figure 13), contrary to observation. Although the hydrogen bonds in the chains of F4BImNN bring the donor N−H groups into close proximity with the large spin populations on the nitronylnitroxide N−O units, the spin densities on the N−H unit are quite small (Figure 2) and apparently do not provide effective exchange linkage between the radicals. A similar situation occurs in some benzimidazole *tert*-butylnitroxides,[4d] where very close N−H···O−N contacts hold pairs of radicals together, but the dominant exchange path occurs by direct dipolar interaction between nitroxide units, instead of through the small spin densities of N−H.

The FM SP model of Figure 13 gives a good account of the dominant J_{chain} 1-D chain exchange in F4BImNN. The weaker

(22) Takeda, K.; Hamano, T.; Kawae, T.; Hidaka, M.; Takahashi, M.; Kawasaki, S.; Mukai, K. *J. Phys. Soc. Jpn.* **1995**, *64*, 2343.
(23) (a) Mouritsen, O. G.; Kjaersgaard Hansen, E.; Knak Jensen, S. J. *Phys. Rev. B* **1980**, *22*, 3256. (b) Becerra, C. C.; Oliveira, N. F., Jr.; Paduan-Filho, A.; Figueiredo, W.; Souza, M. V. P. *Phys. Rev. B* **1988**, *38*, 6887. (c) Kobayashi, T.; Takiguchi, M.; Amaya, K.; Sugimoto, H.; Kajiwara, A.; Harada, A.; Kamachi, M. *J. Phys. Soc. Jpn.* **1993**, *62*, 3239. (d) Takeda, K.; Hamano, T.; Kawae, T.; Hidaka, M.; Takahashi, M.; Kawasaki, S.; Mukai, K. *J. Phys. Soc. Jpn.* **1995**, *64*, 2343. (e) Takeda, K.; Mita, M.; Kawae, T.; Takumi, M.; Nagata, K.; Tamura, M.; Kinoshita, M. *J. Phys. Chem. B* **1998**, *102*, 671. (f) Takeda, K.; Yoshida, Y.; Inanaga, Y.; Kawae, T.; Shiomi, D.; Ise, T.; Kozaki, M.; Okada, K.; Sato, K.; Takui, T. *Phys. Rev. B* **2005**, *72*, 024435/1. (g) Peres, N. M. R. *J. Phys.: Condens. Matter* **2003**, *15*, 7271.
(24) de Jongh, L. J.; Miedema, A. R. *Adv. Phys.* **1974**, *23*, 1.
(25) Miyazaki, Y.; Matsumoto, T.; Ishida, T.; Nogami, T.; Sorai, M. *Bull. Chem. Soc. Jpn.* **2000**, *73*, 67.
(26) Ohmae, N.; Kajiwara, A.; Miyazaki, Y.; Kamachi, M.; Sorai, M. *Thermochim. Acta* **1995**, *267*, 435.

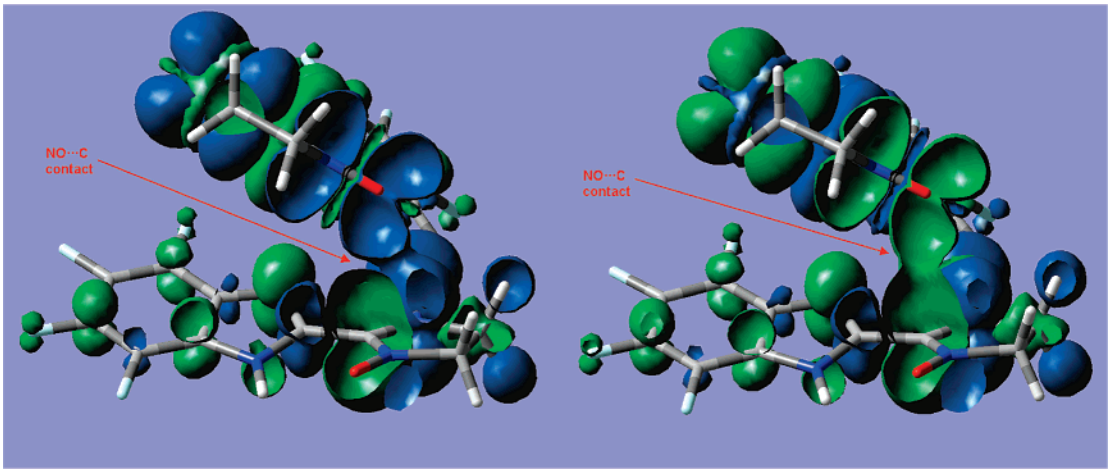

Figure 12. Spin density surfaces for F4BImNN radicals in a stack for high spin FM (left) and low spin AFM coupled (right) states, z-clipped at a plane including the N−O···C contact. Green and blue surfaces denote opposite spin density sign. Picture from GaussView 3.07 using an surface isovalue of 0.0004.

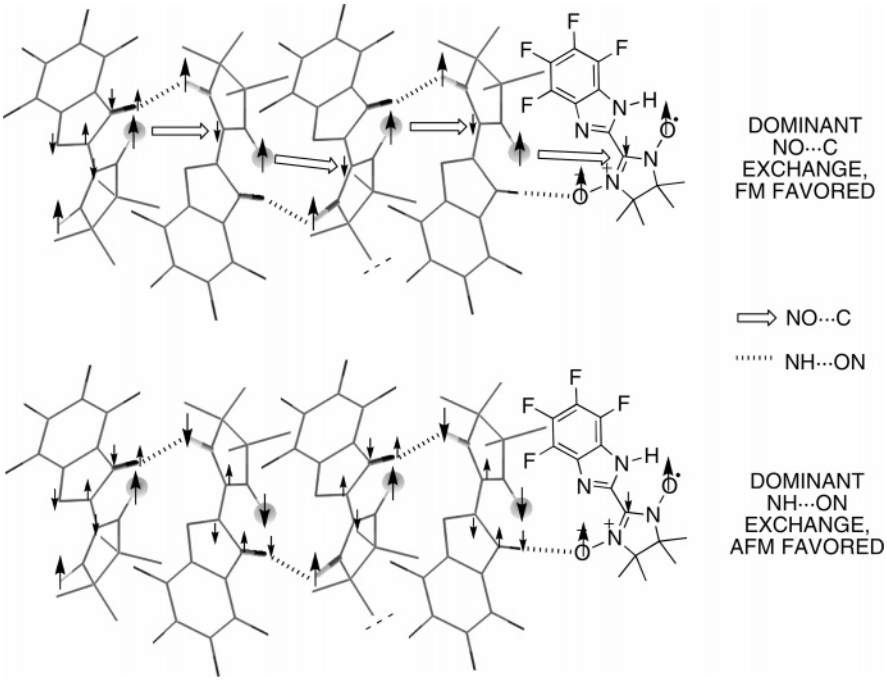

Figure 13. Possible spin polarization (SP) exchange pathways in F4BImNN. N−H···O−N contacts shown as dashed lines; N−O···C contacts shown as arrows. Qualitative spin polarizations taken from Figure 2.

interchain exchange J_{inter} that leads to bulk ordering is harder to assign. There are numerous intermolecular contacts of ≤3.7 Å involving the nitroxide oxygen atoms in F4BImNN, but almost all of these are within the 1-D chains shown in Figures 5 and 13. For example, Figure 14 shows interchain (N4)O2···(H)C5 nitroxide NO to nitroxide methyl contacts (r((N4)O2···H5B(C5)) = 3.68 Å, r(O2···C5) = 4.294(6) Å) that link the 1-D chains to form 2-D sheets in the crystallographic *ac*-plane. These are shown in Figure 14: the hydrogen-bonded chains run into the plane of the figure along the *c*-axis, and the (N4)-O2···(H)C5 contacts are in the middle, roughly along the *a*-axis. The nitroxide methyl groups have only small spin densities from Figure 2 but could provide pathways for weak exchange.

A third dimension of intermolecular contacts occurs between nitroxide NO groups and peripheral benzenoid CF and nitroxide methyl groups on a neighboring 2-D sheet. Each NO group is 4.4−4.5 Å from two CF groups and one methyl CH. These

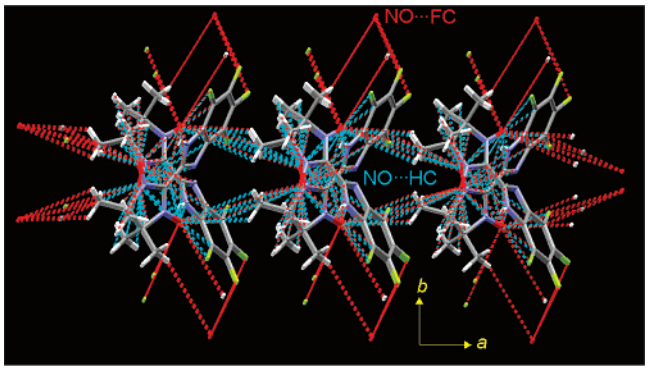

Figure 14. Nitroxide to F−C and nitroxide to methyl contacts between hydrogen-bonded chains in F4BImNN; chains run along the *c*-axis into the figure.

contacts are labeled in Figure 14 as NO···FC contacts, as red dashed lines roughly along the *b*-axis, on the upper and lower

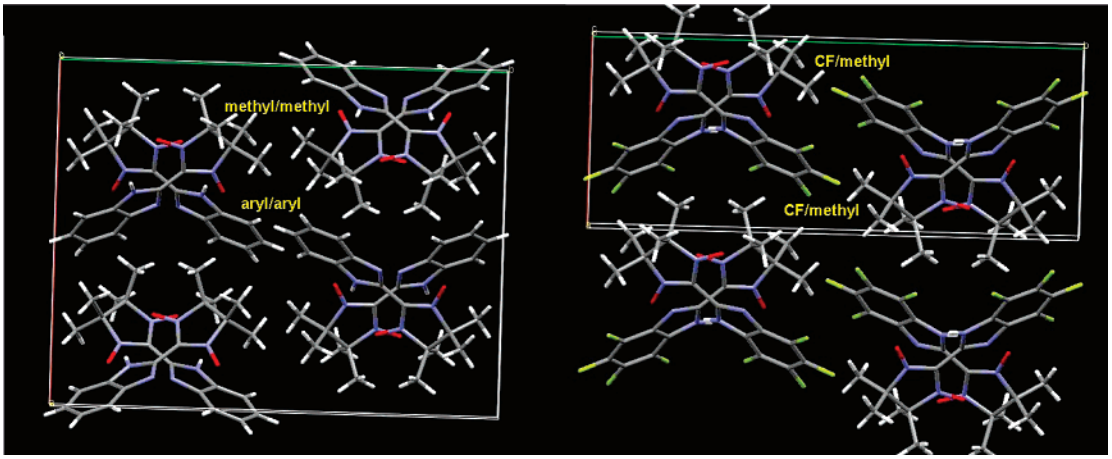

Figure 15. Contacts between hydrogen-bonded chains in BImNN (left, CSD deposition code REFXUV) and F4BImNN, showing unit cells; chains run into the figure.

peripheries of the figure. The exchange role of the CF groups is not obvious, but the computational data from Figure 2 indicate up to 0.1% of a spin resides on the fluorines to provide additional exchange possibilities. We must emphasize that the suggested electronic exchange roles for the NO···HC and NO···FC contacts shown in Figure 14 are speculative at present, but there appear to be no closer intermolecular exchange contacts between sites of a larger spin density.

Assuming *a priori* that neither BImNN nor F4BImNN undergoes significant changes in crystallographic packing upon cooling to below a few kelvins, the difference between the two is the packing *between* the 1-D stacked chains. The CF units in F4BImNN form favorable *CF*/*methyl* contacts with nitronylnitroxide methyl groups, bringing the benzenoid rings into closer proximity to the nitronylnitroxide units than occurs in BImNN, for which *methyl*/*methyl* and *aryl*/*aryl* contacts dominate interchain contacts. Figure 15 shows comparison views of the regions of interchain contact. The chains in the two molecules are geometrically "offset" in different ways, despite their very similar *intrachain* crystallography.

This difference raises the question of whether or how the radicals' magnetisms fundamentally differ. Above 2 K there is little difference in magnetic behavior, consistent with the dominant 1-D ferromagnetic SP exchange pathway created by the intrachain similarity. But, the present study clearly shows that F4BImNN orders below 0.7 K. Analogous behavior has not been reported for BImNN, although Sugano et al.[7a] estimated that $zJ_{inter} = 0.24$ K based on susceptibility measurements over 1.8−5 K. Using eq 4 with $zJ_{inter} = 0.24$ K and $J_{chain} = (+)22$ K from the work of Sugano et al. would predict an ordering temperature slightly above 1 K for BImNN. Barring clearer evidence of bulk ordering in BImNN, it is not possible to tell whether the interchain geometry differences between it and F4BImNN correlate with significant differences in their low-temperature magnetic behavior.

Conclusions

F4BImNN is a quasi 1-D organic ferromagnet that exhibits strong 1-D FM chain exchange attributable to favorable spin polarization induced inter-radical interactions along hydrogen-bonded chains. Variable temperature solid-phase ESR spectroscopy shows *g*-value shifts and line shape changes consistent with dominant 1-D axial exchange interactions in the solid. Heat capacity measurements are also consistent with the quasi 1-D nature of the exchange interactions. Both magnetic susceptibility and heat capacity measurements at zero field indicate a critical temperature of $T_c = 0.7$ K. The variation of magnetic heat capacity of F4BImNN with applied magnetic field is consistent with an ordering transition to a bulk antiferromagnetic ground state below T_c. The quasi-1D ferromagnetic chain exchange is fairly strong for an organic system, $J_{chain} \approx +22$ K; the low temperature heat capacity variation as a function of temperature allows a rough estimate of a ratio of intrachain to interchain exchange, $|J_{chain}/zJ_{inter}| \approx 220-250$.

The use of benzimidazole-based hydrogen bonding to assemble F4BImNN into a piled stack motif was a crucial strategic choice in finding this addition to the family of pure organic systems that exhibit bulk magnetic ordering. Further use of hydrogen-bonding strategies seems promising to find additional organic materials with magnetic ordering.

Acknowledgment. This work was supported in part by the U.S. National Science Foundation by grants CHE 0415716 (H.M., Z.D., P.M.L.), CHE-9974648 (UMass-Amherst X-ray Structural Characterization facility), CTS-0116498 (UMass-Amherst Nanomagnetic Characterization Facility), and CHE-0443180 (UMass-Amherst Electron Paramagnetic Resonance Facility). Support was also provided by the Fundação de Amparo à Pesquisa do Estado de São Paulo (FAPESP) in Brazil (A.P.F., V.B., N.F.O.). We thank Dr. Gregory Dabkowski of the University of Massachusetts Amherst Microanalytical Laboratory for elemental microanalyses.

Supporting Information Available: Complete ref 16, F4BImNN crystallographic summary and HPLC trace, F4BImNN computed spin density, computed F4BImNN dyad triplet-single energy gap in crystallographic chain. This information is available free of charge on the Internet at http://pubs.acs.org.

JA074211G